Investigation of Antibacterial Activity and Related Mechanism of a Series of Nano-Mg(OH)$_2$

Xiaohong Pan,[†,‡] Yonghao Wang,[†] Zhi Chen,[†,‡] Danmei Pan,[†] Yangjian Cheng,[†] Zunjing Liu,[†] Zhang Lin,*[,†] and Xiong Guan*[,‡]

[†]State Key Laboratory of Structural Chemistry, Fujian Institute of Research on the Structure of Matter, Chinese Academy of Sciences, Fuzhou, Fujian, 350002, P. R. China

[‡]Key Lab of Biopesticide and Chemical Biology, Fujian Agriculture and Forestry University, Ministry of Education, Fuzhou, Fujian 350002, P. R., China

Ⓢ *Supporting Information*

ABSTRACT: Here we reported the antibacterial effect and related mechanism of three nano-Mg(OH)$_2$ slurries using *Escherichia coli* as model bacteria. X-ray diffraction (XRD), scanning electron microscopy (SEM) and laser particle size analysis revealed that the as-synthesized Mg(OH)$_{2\_MgCl2}$, Mg(OH)$_{2\_MgSO4}$ and Mg(OH)$_{2\_MgO}$ are all composed by nanoflakes with different sizes, and their aggregates in water are 5.5, 4.5, and 1.2 μm, respectively. Bactericidal tests showed that the antibacterial efficiency is conversely correlated with the size of Mg(OH)$_2$ aggregates. Transmission electron microscopy (TEM) observation have not provided evidence of cellular internalization, however, the antibacterial effect is positive correlation to the loss of integrity of cell walls. SEM and zeta potential analysis revealed that the adhering ability of Mg(OH)$_2$ on the bacterial surface is Mg(OH)$_{2\_MgCl2}$ > Mg(OH)$_{2\_MgSO4}$ > Mg(OH)$_{2\_MgO}$, indicating the toxicity of Mg(OH)$_2$ may be caused by the electrostatic interaction-induced external adsorption. Confocal laser scanning microscopy (CLSM) further revealed that the adhering of Mg(OH)$_2$ on the bacterial surface could increase the permeability of cell membranes. Taken together, the antibacterial mechanism of nano-Mg(OH)$_2$ could be as follows: nano-Mg(OH)$_2$ adsorbed on the bacterial surface by charge attraction first, and then destroyed the integrity of cell walls, which resulting in the final death of bacteria.

External adsorption induce antibacterial mechanism of nano-Mg(OH)$_2$

KEYWORDS: *Mg(OH)$_2$ nanoparticles, antibacterial activity, surface charges, microscopic, Escherichia coli, permeability*
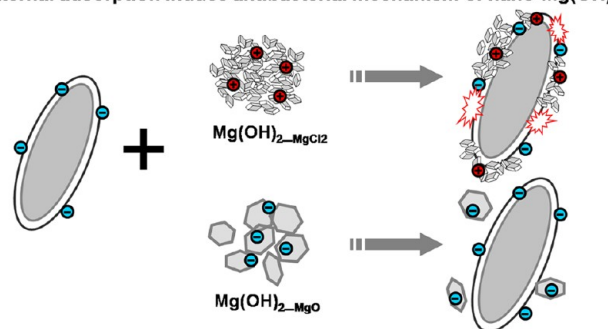
■ INTRODUCTION

Nanomaterials are widely used in the removal of organic matter or heavy metal in industrial wastewater due to their small size and relative large specific surface area.[1,2] For instance, zerovalent iron and iron oxide material were used to effectively remove heavy metal ions (As, Cr) and nitrates from wastewater.[3−5] Recently, not only the toxicological effects of nanomaterials, but also the antibacterial activity have raised researchers' concerns and interesting. It has been reported that the nanoscale TiO$_2$ was apt to cause lung inflammation,[6] and ZnO nanoparticles showed strong toxicity to bacteria, aquatic, and terrestrial organisms.[7−9] However, TiO$_2$ and ZnO have also been recognized as antibacterial agents.[10,11] Therefore, it is a hot research topic to develop new antibacterial materials that are not toxicity.

As a low cost and environmentally friendly material, nano-Mg(OH)$_2$ has already been widely applied in the process of neutralizing acid water and dye from wastewater.[12−15] Over the past decade, the global consumption of Mg(OH)$_2$ in wastewater treatment is more than 48 000 tons annually.[16] At present, the commercial Mg(OH)$_2$ mainly involves three states, including slurry, filter cake, and powder.[17] Among these states, the slurry-like Mg(OH)$_2$ has been most frequently used because of its excellent dispersibility and fluidity, as well as strong adsorption ability. However, little attention was paid to the cytotoxicity and antibacterial activity of nano-Mg(OH)$_2$. Recently, Dong et al. studied the interaction of electrolytic nano-Mg(OH)$_2$ suspension to *E. coli*. It revealed the nano-Mg(OH)$_2$ has antibacterial effect, and the mechanism might be the direct contact between bacterial cells and nanoplatelets.[18,19] As we know, there are various synthetic methods of nano-Mg(OH)$_2$, including electrolytic method, hydration of MgO,[20] or precipitation of a magnesium salt with an alkaline solution.[21,22] Different synthetic methods may result in different size, morphology, aggregation state, and surface charge of Mg(OH)$_2$. Accordingly, the resulted material may

have different antibacterial effects. Therefore, for the appropriate selection of nano-Mg(OH)$_2$ as antibacterial agents, it is necessary to systematically evaluate the related antibacterial mechanism of nano-Mg(OH)$_2$.

In this work, we synthesized three typical nano-Mg(OH)$_2$ slurries by alkaline precipitation of magnesium salts and hydration of MgO. Then Gram-negative *Escherichia coli* was used as model bacterial species to evaluate the antibacterial activity of the Mg(OH)$_2$ slurries. In depth, the relationship between antibacterial effects with particle size, aggregated morphology, surface charge of the materials, as well as the contacting degree between the material and bacteria were all studied. It is worth noting that we first provide the comprehensive experimental data to explore the antibacterial mechanism of a series of nano-Mg(OH)$_2$. We expected that this study can offer significant reference for the selection of Mg(OH)$_2$ in the real application.

■ MATERIALS AND METHODS

Mg(OH)$_2$ Nanoparticles. Nano-Mg(OH)$_2$ slurries (purity of over 97%) were prepared with following procedures: (a) coprecipitation of magnesium chloride hexahydrate and sodium hydroxide in double-distilled water (ddH$_2$O) under room temperature[22] (named as Mg(OH)$_{2\_MgCl2}$); (b) coprecipitation of anhydrous magnesium sulfate in ammonia under room temperature[22] (named as Mg(OH)$_{2\_MgSO4}$); (c) hydration of MgO: 2 g of MgO was heated at 600 °C for 2 h, and then the powder was immediately quenched in 500 mL ddH$_2$O, and the mixture was stirred for 24 h (named as Mg(OH)$_{2\_MgO}$). All the suspensions were washed with ddH$_2$O three times by centrifugation at 10 000 g for 10 min. The pH values of all synthesized 1 mg/mL Mg(OH)$_2$ slurries are around 10.3.

Characterization of Nano-Mg(OH)$_2$. The morphology and size of the synthesized nano-Mg(OH)$_2$ samples (the concentration was 1 mg/mL) were characterized on a JSM-6700F scanning electron microscope (SEM) [JEOL Ltd., Japan] equipped with an Oxford-INCA energy-dispersive X-ray spectroscopy (EDS). Samples were identified by X-ray diffraction (XRD) pattern using a PANalytical X'Pert PRO diffractometer with Cu Kα radiation (40 kV, 40 mA) in a continuous scanning mode. The 2θ scanning ranged from 5° to 85° in steps of 0.017° with a collection time of 20 s per step. The average crystallite size was determined from the peak broadening according to the Scherrer equation. In addition, the aggregate size distribution was characterized by the Winner 2308 laser particle size analyzer [Jinan Winner Particle Technology Co., Ltd.].

Bacterial Culture Conditions and Antibacterial Test. *E. coli* was cultured in Luria−Bertani (LB) medium (NaCl 10 g/L, tryptone 10 g/L, yeast extract 5 g/L, pH 7.0) at 37 °C with aeration, and the shaking speed was set at 180 rpm. After 24 h, bacteria were centrifuged at 5,000 g for 5 min, and then the pellet was washed with ddH$_2$O for three times, finally suspended in the ddH$_2$O. For the cytotoxicity assays, certain amount of nano-Mg(OH)$_2$ was added to 10 mL bacterial suspension to obtain the exposure concentrations of 0.1, 0.3, and 0.5 mg/mL, respectively. Then the mixture of bacteria and nanoparticles was shaken at 37 °C in dark. Subsequently, 100 μL diluted suspension was streaked on agar medium, and then the plate was incubated at 37 °C for 24 h. The inhibition of bacterial growth was evaluated by the colony-forming units (CFUs). Our control experiment was conducted in the ddH$_2$O and adjusted the pH of bacterial suspension (without nanoparticles) around 9−10. The inhibition rate of bacteria was calculated as follows

$$\text{lethality rate} = (1 - N1/N2) \times 100\%$$

Where N1 is the colony number after the exposure to nanoparticles, and N2 indicates the colony number of control. All experiments were performed in triplicate.

Microscopic Investigation of Bacteria. After the exposure, bacteria were fixed with 2% glutaraldehyde for 24 h. Samples were

postfixed with 1% osmic acid for 2 h, and then fixed samples were dehydrated in an acetone gradient (35, 50, 70, 80, 95, and 100%) for 3 min, respectively. Finally, air-dried samples were observed on JSM-6700F SEM. The sample preparation of transmission electron microscopy (TEM) was the same as SEM from the steps of harvest to dehydration, and then cells were embedded in resin. Ultrathin sections were prepared and counterstained with Leica's and uranyl acetate onto a copper grid. Grids were conducted on a JEM-2010 TEM [JEOL Ltd., Japan] at 200 kV.

Zeta-Potential Measurement. The changes of surface charge after the exposure of Mg(OH)$_2$ nanoparticles to bacteria were determined by a ZetaPlus Zeta Potential Analyzer produced by Malvern Instruments Corporation. The concentration of nanoparticles was 0.1, 0.3, and 0.5 mg/mL which were synthesized by three different methods. For each sample, an appropriate amount of undiluted solution was placed into the cuvette, and an average zeta potential value was obtained from three individual measurements. The solution media was set as water for all zeta potential measurements.

Cellular Staining with Fluorescent Probes and High Epifluorescence Microscopy. Apoptotic Cell Hoechst 33342/PI Detection Kit was used in our experiment. The collected bacteria were resuspended in 1 mL LB medium and then incubated with 10 μL Hoechst 33342 at 37 °C for 10 min (λ ex 355 nm, λ em 465 nm, and the final concentration was 5 μg/mL). Subsequently, the bacterial suspension was centrifuged at 5,000 g for 5 min at 4 °C, and the supernatant was discarded. Then the samples were resuspended in 1.0 mL Buffer A and incubated with 5 μL propidium iodide (PI) for 10 min in dark (λ ex 540 nm, λ em 620 nm, and the final concentration of PI was 5 μg/mL). The unincorporated dyes were removed by washing with Buffer A. One droplet of cell suspension (5 μL) was dropped on the freshly treated glass slide, and then it was covered with the coverslip without bubbles. Finally, the glass piece was sealed using the petroxolin. The samples were recorded using a laser scanning confocal microscope [FV1000 CLSM, OLYMPUUS, Japan].

■ RESULTS AND DISCUSSION

Characterization of nano-Mg(OH)$_2$. The as-synthesized Mg(OH)$_2$ slurries were quickly dried into powder and then identified by XRD. Figure 1 indicates that all diffraction peaks could be well indexed as hexagonal magnesium hydroxide
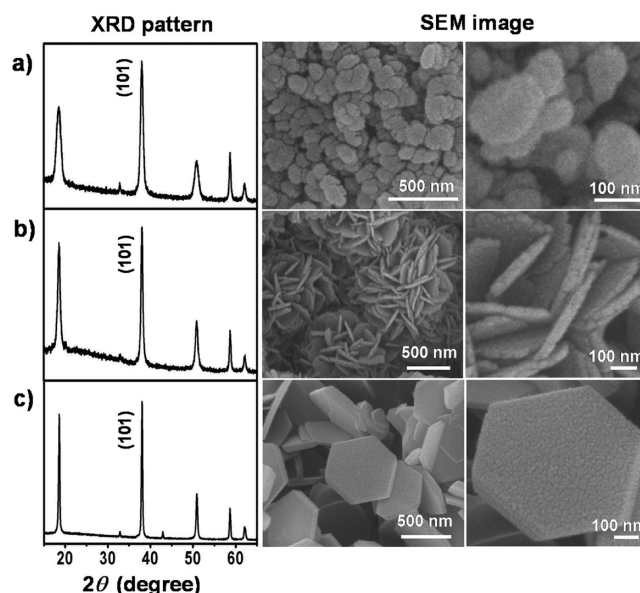

Figure 1. XRD patterns and SEM images were used to confirm the crystalline structures and observe the morphology of as-synthesized Mg(OH)$_2$ samples respectively. (a−c) Samples of Mg(OH)$_{2\_MgCl2}$, Mg(OH)$_{2\_MgSO4}$, and Mg(OH)$_{2\_MgO}$, respectively.

structure (JCPDF044−1482). According to the Scherrer equation, the size of $Mg(OH)_{2\_MgCl2}$, $Mg(OH)_{2\_MgSO4}$ and $Mg(OH)_{2\_MgO}$ planes at (101) direction was 12.9 ± 0.7, 21.4 ± 1.8, and 44.8 ± 8.1 nm, respectively. This means that three types of $Mg(OH)_2$ particles in some dimension were at nanolevel. However, SEM observation revealed that the as-synthesized nano-$Mg(OH)_2$ are not only with different original morphology, but are very easily aggregated into microparticles. The $Mg(OH)_{2\_MgCl2}$ sample contains a lot of small flakes around tens of nanometer, which further aggregated densely. $Mg(OH)_{2\_MgSO4}$ had the flower-like self-supported structure consisted of cross nanosheets. The $Mg(OH)_{2\_MgO}$ consisted of the micrometer-scale hexagonal nanoplates. Since $Mg(OH)_2$ slurries are actually wet instead of as dry powder, we further use laser particle size analysis to monitor the agglomeration state of nano-$Mg(OH)_2$ in water (details were showed in Supporting Information, Part I, Figure S1). All the $Mg(OH)_2$ particles were dispersed by ultrasonic method before mixing with E. coli, but the results of laser particle size analysis showed that the average particle size of $Mg(OH)_{2\_MgCl2}$, $Mg(OH)_{2\_MgSO4}$, and Mg-$(OH)_{2\_MgO}$ is 5.5, 4.5, and 1.2 μm, respectively. Above analysis revealed that though synthesized as nanoparticles with different shape and size, all these samples are easily aggregated into micrometer level during usage as slurry in water.

Toxicological Effect of Nano-$Mg(OH)_2$ on E. coli. Because $Mg(OH)_2$ is slightly soluble in water with solubility constant of 5.61×10^{-12}, and the pH of $Mg(OH)_2$ suspension in water is around 10,[18,19] thus we choose the alkaline resistance E. coli for studying the antibacterial effect of nano-$Mg(OH)_2$ (Our previous study indicated that this bacterium had a good resistance of alkalinity even in a circumstance with pH value of 11, details please see the Support Information, Part II, Figure S2).The antibacterial activity was evaluated by regrowing the E. coli on solid agar plate after exposing with 0.1, 0.3, and 0.5 mg/mL $Mg(OH)_2$ respectively. As shown in Figure 2, $Mg(OH)_{2\_MgCl2}$ had the significant antibacterial activity toward E. coli when its concentration was 0.1 mg/mL, and the inhibition rate was around 88%, whereas the antibacterial effect of $Mg(OH)_{2\_MgSO4}$ and $Mg(OH)_{2\_MgO}$ was not obvious at the same concentration. However, when the concentration increased to 0.3 mg/mL, the $Mg(OH)_{2\_MgSO4}$ caused the inhibition of 60% for E. coli. Only when the concentration

increased to 0.5 mg/mL, the $Mg(OH)_{2\_MgO}$ exerted the comparative antibacterial efficiency with a inhibition rate of merely 53%. Overall, the antibacterial activity sequence of $Mg(OH)_2$ toward E. coli was $Mg(OH)_{2\_MgCl2}$ > Mg-$(OH)_{2\_MgSO4}$ > $Mg(OH)_{2\_MgO}$.

Cause of the Toxicology of Nano-$Mg(OH)_2$ toward E. coli. Previous reports showed that the bacterial toxicity could be attributed to the following reasons: (i) cellular internalization of nanoparticles;[23−25] (ii) direct surface interaction;[18,19] (iii) the dissolution metal ions of nanoscale metal oxide.[8,26−28] Commonly, if the antibacterial effect is originated from the size effect of the material (that is the cellular internalization), the smaller the size, the stronger the inhibition effect.[29,30] However, combined with the result from laser particle size analysis, we found the $Mg(OH)_{2\_MgCl2}$ that with the largest average particle size has the strongest antibacterial effect. The $Mg(OH)_{2\_MgO}$ with the smallest size distribution has the weakest antibacterial effect. Thus we considered the size effect was not the major factor on antibacterial effect in this study. For verifying this, we performed the TEM thin-sections of bacteria coupled with EDS to study the distribution of Mg element inside the bacteria after interacting with $Mg(OH)_2$. No signal of Mg element was detected from the EDS analysis in several randomly selected areas. This indicated that the $Mg(OH)_2$ particles and dissolved Mg elements might not enter into the bacterial interior. However, an obvious changes of cell walls were observed after exposure with $Mg(OH)_2$. As shown in Figure 3a, bacteria without being exposed to $Mg(OH)_2$ exhibited relatively intact profile and clear cell walls. After interacting with 0.5 mg/mL $Mg(OH)_{2\_MgCl2}$ for 4 h, the entire profile became unclear, and most of the cell walls were damaged. When exposed to $Mg(OH)_{2\_MgSO4}$, the damaged level of the bacterial profile as well as the cell wall decreased at some certain comparing to $Mg(OH)_{2\_MgCl2}$. When exposed to $Mg(OH)_{2\_MgO}$, the entire profile and cell wall still remained complete. Thus the toxicity of $Mg(OH)_2$ may be caused by the external adsorption rather than the cellular internalization, which induced the disorganization of cell walls.

In addition, SEM analysis was used to investigate the distribution of $Mg(OH)_2$ material on bacterial surfaces. Figure 3b shows that after treated by $Mg(OH)_{2\_MgCl2}$, the bacterial surfaces were no longer smooth. Instead, there were a lot of loose materials attached on the bacterial surface. EDS spectrum revealed that these aggregates contained Mg element, showing that a number of $Mg(OH)_{2\_MgCl2}$ nanoparticles gathered on the surface of E. coli. As to bacteria that treated with $Mg(OH)_{2\_MgSO4}$ sample, similarly, analysis revealed that $Mg(OH)_{2\_MgSO4}$ may attach on the bacterial surface, however, the attached amount is not as much as $Mg(OH)_{2\_MgCl2}$ treated bacteria. As to $Mg(OH)_{2\_MgO}$ treated sample, the bacterial surface is almost as smooth as the control sample. We further noticed the dispersed hexagonal nanoplates $Mg(OH)_{2\_MgO}$, which were not closely attached to the bacterial surface at all (shown by circle in Figure 3b). This result indicated that the three $Mg(OH)_2$ samples have different adhering ability on the bacterial surfaces, that is $Mg(OH)_{2\_MgCl2}$ > $Mg(OH)_{2\_MgSO4}$ > $Mg(OH)_{2\_MgO}$. This sequence seems directly correlation to the antibacterial efficiency of the material.

Analysis of the Toxicological Mechanism. On the basis of above analysis, we considered that the external adsorption may play an important role on the antibacterial effect, which is very similar to Dong's suggestion.[18,19] However, we found the adsorption ability of three samples seems different. We further
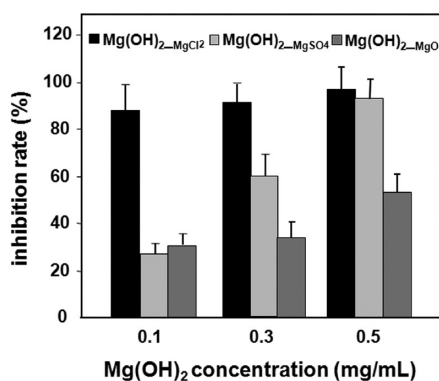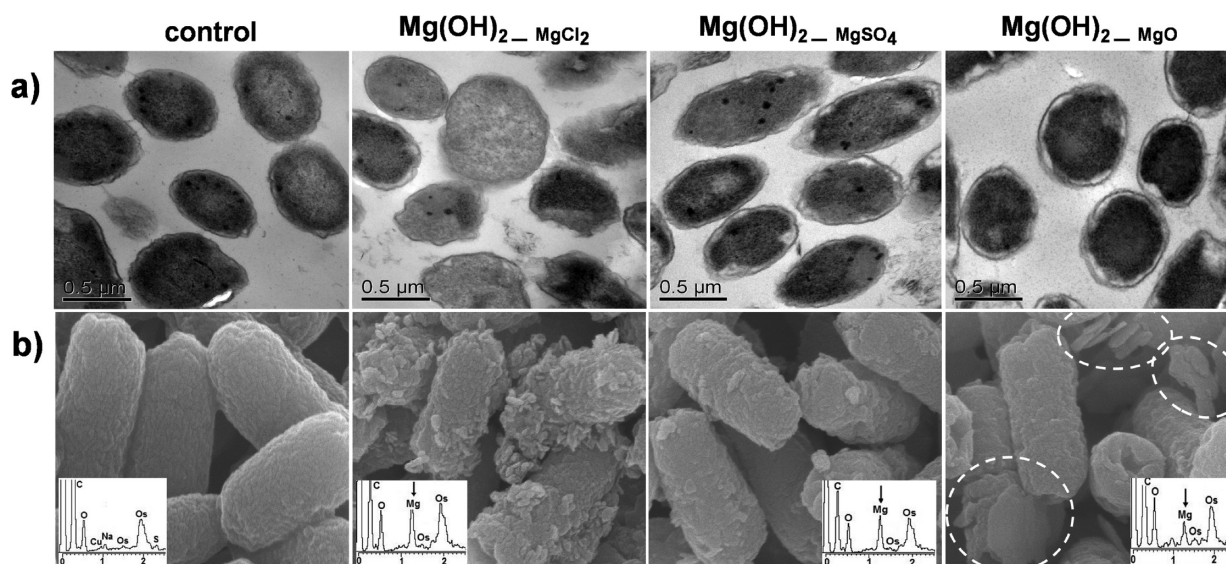
Figure 2. Relationship between the antibacterial efficiency and the $Mg(OH)_2$ species. E. coli was exposed for 4 h to 0.1, 0.3, and 0.5 mg/ mL of different types of $Mg(OH)_2$. Comparison with a positive control (bacteria in ddH_2O at pH ~10 without nanoparticles) permitted to determine the percentage of antibacterial efficiency. Data presented as mean ± standard deviation (n = 3).

Figure 3. (a) TEM and (b) SEM images of *E. coli* treated with 0.5 mg/mL Mg(OH)$_2$ slurries for 4 h, respectively. Inset images of b show the EDS analysis of bacteria. The size of all SEM images is 6.0 μm.

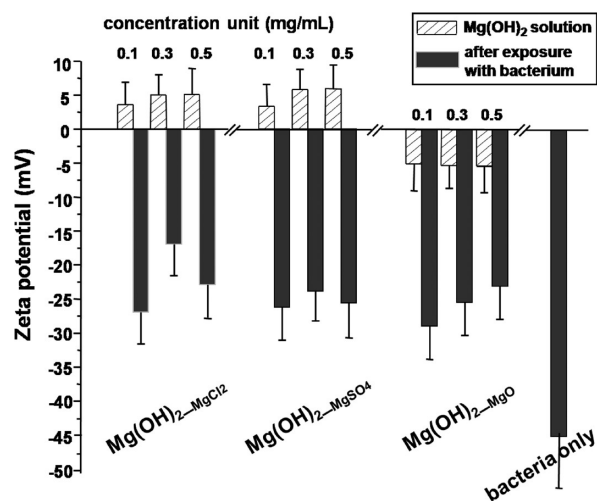explored the zeta potentials of all the samples. As shown in Figure 4, Mg(OH)$_{2\_MgCl2}$ and Mg(OH)$_{2\_MgSO4}$ carried positive

Figure 4. Zeta-potentials of nanoparticles before and after exposure with bacteria for 24 h. Note the negative zeta potential for Mg(OH)$_{2\_MgO}$ without bacteria.

charges, while Mg(OH)$_{2\_MgO}$ carried negative charges. After incubation Mg(OH)$_2$ with highly negatively charged *E. coli*, all the three mixture solutions became negatively charged in zeta potential. This result indicates that the binding of Mg(OH)$_2$ with bacteria could be driven by the electrostatic interactions.[31] In this situation, the positively charged Mg(OH)$_{2\_MgCl2}$ and Mg(OH)$_{2\_MgSO4}$ could be more active for the adsorption process than the negatively charged Mg(OH)$_{2\_MgO}$. This is coincident with the SEM observation. Electrostatic repulsion between Mg(OH)$_{2\_MgO}$ and *E. coli* would result in the loose connection of Mg(OH)$_{2\_MgO}$ on the bacterial surface, and consequently limit its toxicity,[32] although laser particle size analysis revealed the smallest average particle size of this sample. Moreover, we also found that the morphology of the aggregates influence the toxicity. For example, both Mg-(OH)$_{2\_MgCl2}$ and Mg(OH)$_{2\_MgSO4}$ are positively charged, and

with similar particle size distribution (5.5 and 4.5 μm), while the flower-like self-supported structure Mg(OH)$_{2\_MgSO4}$ showed weaker toxicity compare to lump-like aggregates of Mg(OH)$_{2\_MgCl2}$. It revealed that the complex structure of nano-Mg(OH)$_2$ might hinder its contact degree on the bacterial surface. In addition, the pH values of nanoparticles and bacterial suspension were shown in the Supporting Information, Part III, Table S1. The result revealed that the pH was maintained at a stable value, and there is no difference among three samples after exposure with equal nanoparticles. Therefore, we considered that the surface charge of the nano-Mg(OH)$_2$ may be the main reason to induce the different antibacterial effects.

It was suggested that the introducing of Mg(OH)$_2$ nanoparticles may cause considerable damage on the cell membrane of *E. coli*.[17,18] In order to verifying this, we observed the bacteria by fluorescence microscope. Both Hoechst 33342 and PI were used for double-staining the bacteria, for revealing the changes on the permeability of cell membranes. As we known, Hoechst 33342 is cell-permeable, which could bind the DNA of all the cells (live and dead). Thus the healthy cell shows weak blue nuclei,[33] the apoptosis cell appears strong blue nuclei. PI could bind to DNA or RNA and stain only the necrotic cells, thus intracellular staining of PI would show red fluorescence.[33,34] Figure 5a shows that almost all of the control bacteria appears blue nuclei, indicating the PI can not penetrate the cell membranes of viable cells. After exposure with different types of 0.5 mg/mL Mg(OH)$_2$ nanoparticles for 24 h, the stained situations were obviously different. As shown in Figure 5b, Mg(OH)$_{2\_MgCl2}$-treated bacteria were almost red with fluorescence, indicating the highly permeability of PI dye toward Mg(OH)$_{2\_MgCl2}$-treated bacteria, and most of the cells were dead. The Mg(OH)$_{2\_MgSO4}$-treated bacteria show strong blue and red nuclei, revealing that the PI permeability of Mg(OH)$_{2\_MgSO4}$-treated bacteria decreased compared to Mg-(OH)$_{2\_MgCl2}$-treated bacteria. The strong blue and red fluorescence also indicated that Mg(OH)$_{2\_MgSO4}$ induced the apoptosis for the most bacteria, and part of the bacteria became necrosis (as shown in Figure 5c). Figure 5d reveals that Mg(OH)$_{2\_MgO}$-treated cells showing weak blue nuclei, which
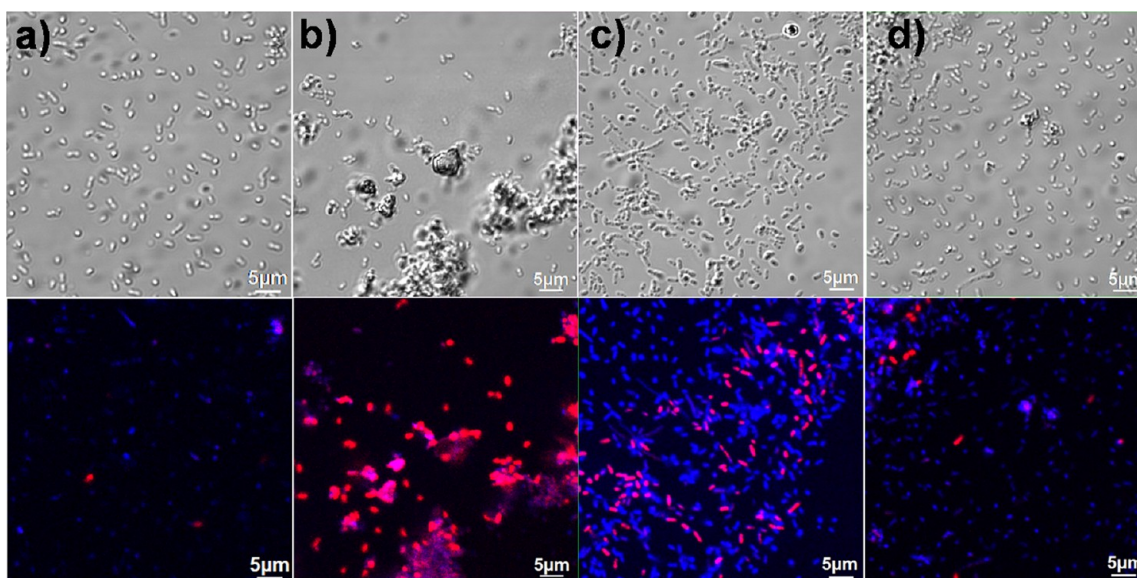
Figure 5. Microscopy investigation of apoptotic and necrotic cells morphology after Mg(OH)$_2$ exposure. 0.5 mg/mL nanoparticles were added to the bacterial solution for 24 h. All stained samples were imaged at comparable cell concentration. (a) Control, (b) Mg(OH)$_{2\_MgCl2}$, (c) Mg(OH)$_{2\_MgSO4}$, and (d) Mg(OH)$_{2\_MgO}$. Note the higher extent of cell lysis and aggregation of dead cells with Mg(OH)$_{2\_MgCl2}$ exposure.

indicated Mg(OH)$_{2\_MgO}$ had a weak destructive effect on the cell membranes and majority of bacteria were viable, and thus the PI dye to penetrate the cell. In summary, the bacterial loss of viability is correlated to an impairment of cell membranes integrity, which is highly consistent with the damage degree of cell walls for the three samples by TEM analysis.

Taken together, as shown in Figure 6, we concluded that the antibacterial mechanism of nano-Mg(OH)$_2$ to bacteria may be
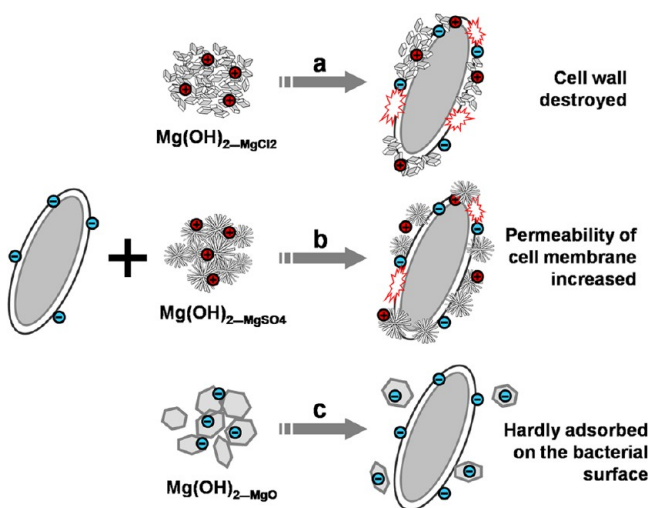

Figure 6. Schematic diagram showed the different contacting patterns between nanoparticle aggregates and bacteria.

induced via two steps. First, with the assistance of electrostatic attractive interactions, positively charged nano-Mg(OH)$_2$ are easily adsorbed onto the bacterial surfaces with negative charge. For the Mg(OH)$_2$ aggregates with the similar size and charge situation, the morphology also affected the contact degree. Second, the adsorbed nanoparticles destroyed the integrity of cell walls, then increased the permeability of cell membranes and finally induced the death of bacteria. In addition, we also found that Mg(OH)$_{2\_MgSO4}$ appeared equivalent inhibition

effect with widely researched ZnO nanoparticles (they had the similar size at [101] direction, as discussed in the Suporting Information Part IV, Figure S3). Therefore, the Mg(OH)$_2$ nanoplatelets have great application potential as a new antibacterial material.

■ ASSOCIATED CONTENT

Ⓢ Supporting Information

Additional figures and table depicting the data in laser particle size analysis, the resistance of alkalinity on *E. coli*, the changes in pH value, and the comparison of inhibition effect between nano-Mg(OH)$_2$ and ZnO. This material is available free of charge via the Internet at http://pubs.acs.org.

■ AUTHOR INFORMATION

Corresponding Author
*E-mail: zlin@fjirsm.ac.cn (Z.L.); guanxfafu@126.com (X.G.). Tel & Fax: (+086)591-83705474 (Z.L.); (+086)591-83789259 (X.G.).

Notes
The authors declare no competing financial interest.

■ ACKNOWLEDGMENTS

■ REFERENCES

(1) Hu, J.; Chen, G. H.; Lo, I. *Water Res.* **2005**, 39, 4528−4536.

(2) Perelshtein, I.; Applerot, G.; Perkas, N.; Wehrschetz-Sigl, E.; Hasmann, A.; Guebitz, G. M.; Gedanken, A. *ACS Appl. Mater. Interfaces* **2008**, *1*, 361−366.

(3) Vlassopoulos, D.; Rivera, N.; O'Day, P. A.; Rafferty, M. T.; Andrews, C. B. *Adv. Arsenic Res.* **2005**, *915*, 344−360.

(4) Ponder, S. M.; Darab, J. G.; Mallouk, T. E. *Environ. Sci. Technol.* **2000**, *34*, 2564−2569.

(5) Su, C. M.; Puls, R. W. *Environ. Sci. Technol.* **2001**, *35*, 4562−4568.

(6) Warheit, D. B.; Reed, K. L.; Sayes, C. M. *Nanotoxicology* **2009**, *3*, 181−187.

(7) Huang, Z. B.; Zheng, X.; Yan, D. H.; Yin, G. F.; Liao, X. M.; Kang, Y. Q.; Yao, Y. D.; Huang, D.; Hao, B. Q. *Langmuir* **2008**, *24*, 4140−4144.

(8) Franklin, N. M.; Rogers, N. J.; Apte, S. C.; Batley, G. E.; Gadd, G. E.; Casey, P. S. *Environ. Sci. Technol.* **2007**, *41*, 8484−8490.

(9) Johnston, B. D.; Scown, T. M.; Moger, J.; Cumberland, S. A.; Baalousha, M.; Linge, K.; Van Aerle, R.; Jarvis, K.; Lead, J. R.; Tyler, C. R. *Environ. Sci. Technol.* **2010**, *44*, 1144−1151.

(10) Yu, J. C.; Ho, W. K.; Lin, J.; Yip, H.; Wong, P. K. *Environ. Sci. Technol.* **2003**, *37*, 2296−2301.

(11) Zhang, L. L.; Jiang, Y. H.; Ding, Y. L.; Povey, M.; York, D. *J. Nanopart. Res.* **2007**, *9*, 479−489.

(12) Booster, J. L.; Van Sandwijk, A.; Reuter, M. A. *Miner. Eng.* **2003**, *16*, 273−281.

(13) Gao, C. L.; Zhang, W. L.; Li, H. B.; Lang, L. M.; Xu, Z. *Cryst. Growth Des.* **2008**, *8*, 3785−3790.

(14) Gao, B. Y.; Yue, Q. Y.; Wang, Y.; Zhou, W. Z. *J. Environ. Manage.* **2007**, *82*, 167−172.

(15) Tan, B. H.; Teng, T. T.; Omar. *Water Res.* **2000**, *34*, 597−601.

(16) Liu, W. Z.; Huang, F.; Wang, Y. J.; Zou, T.; Zheng, J. S.; Lin, Z. *Environ. Sci. Technol.* **2011**, *45*, 1955−1961.

(17) Guo, R. X. *Environ. Prot. Chem. Ind.* **1997**, *17*, 206−210 (in Chinese).

(18) Dong, C. X.; Cairney, J.; Sun, Q. H.; Maddan, O. L.; He, G. H.; Deng, Y. L. *J. Nanopart. Res.* **2010**, *12*, 2101−2109.

(19) Dong, C. X.; Song, D. L.; Cairney, J.; Maddan, O. L.; He, G. H.; Deng, Y. L. *Mater. Res. Bull.* **2011**, *46*, 576−582.

(20) Laska, M.; Valtyni, J.; Fellner, P. *Cryst. Res. Technol.* **1993**, *28*, 931−936.

(21) Hsu, J. P.; Nacu, A. *Colloids Surf., A* **2005**, *262*, 220−231.

(22) Henrist, C.; Mathieu, J. P.; Vogels, C.; Rulmont, A.; Cloots, R. *J. Cryst. Growth* **2003**, *249*, 321−330.

(23) Brayner, R.; Ferrari-Iliou, R.; Brivois, N.; Djediat, S.; Benedetti, M. F.; Fievet, F. *Nano Lett.* **2006**, *6*, 866−870.

(24) Lin, W. S.; Xu, Y.; Huang, C. C.; Ma, Y. F.; Shannon, K. B.; Chen, D. R.; Huang, Y. W. *J. Nanoparticle Res.* **2009**, *11*, 25−39.

(25) Sondi, I.; Salopek-Sondi, B. *J. Colloid Interface Sci.* **2004**, *275*, 177−182.

(26) Heinlaan, M.; Ivask, A.; Blinova, I.; Dubourguier, H. C.; Kahru, A. *Chemosphere* **2008**, *71*, 1308−1316.

(27) Miao, A. J.; Schwehr, K. A.; Xu, C.; Zhang, S. J.; Luo, Z. P.; Quigg, A.; Santschi, P. H. *Environ. Pollut.* **2009**, *157*, 3034−3041.

(28) Xia, T.; Kovochich, M.; Liong, M.; Madler, L.; Gilbert, B.; Shi, H. B.; Yeh, J. I.; Zink, J. I.; Nel, A. E. *ACS Nano* **2008**, *2*, 2121−2134.

(29) Choi, O.; Hu, Z. *Environ. Sci. Technol.* **2008**, *42*, 4583−4588.

(30) Pan, Y.; Neuss, S.; Leifert, A.; Fischler, M.; Wen, F.; Simon, U.; Schmid, G.; Brandau, W.; Jahnen-Dechent, W. *Small* **2007**, *3*, 1941−1949.

(31) Chen, P. Y.; Powell, B. A.; Mortimer, M.; Ke, P. C. *Environ. Sci. Technol.* **2012**, *46*, 12178−12185.

(32) Simon-Deckers, A.; Loo, S.; Mayne-L'Hermite, M.; Herlin-Boime, N.; Menguy, N.; Reynaud, C.; Gouget, B.; Carriere, M. *Environ. Sci. Technol.* **2009**, *43*, 8423−8429.

(33) George, S.; Pokhrel, S.; Xia, T.; Gilbert, B.; Ji, Z. X.; Schowalter, M.; Rosenauer, A.; Damoiseaux, R.; Bradley, K. A.; Madler, L.; Nel, A. E. *ACS Nano* **2010**, *4*, 15−29.

(34) Zhao, Y. Y.; Tian, Y.; Cui, Y.; Liu, W. W.; Ma, W. S.; Jiang, X. Y. *J. Am. Chem. Soc.* **2010**, *132*, 12349−12356.